ARTICLE

doi:10.1038/nature09994

Quantum simulation of antiferromagnetic spin chains in an optical lattice

Jonathan Simon[1], Waseem S. Bakr[1], Ruichao Ma[1], M. Eric Tai[1], Philipp M. Preiss[1] & Markus Greiner[1]

Understanding exotic forms of magnetism in quantum mechanical systems is a central goal of modern condensed matter physics, with implications for systems ranging from high-temperature superconductors to spintronic devices. Simulating magnetic materials in the vicinity of a quantum phase transition is computationally intractable on classical computers, owing to the extreme complexity arising from quantum entanglement between the constituent magnetic spins. Here we use a degenerate Bose gas of rubidium atoms confined in an optical lattice to simulate a chain of interacting quantum Ising spins as they undergo a phase transition. Strong spin interactions are achieved through a site-occupation to pseudo-spin mapping. As we vary a magnetic field, quantum fluctuations drive a phase transition from a paramagnetic phase into an antiferromagnetic phase. In the paramagnetic phase, the interaction between the spins is overwhelmed by the applied field, which aligns the spins. In the antiferromagnetic phase, the interaction dominates and produces staggered magnetic ordering. Magnetic domain formation is observed through both *in situ* site-resolved imaging and noise correlation measurements. By demonstrating a route to quantum magnetism in an optical lattice, this work should facilitate further investigations of magnetic models using ultracold atoms, thereby improving our understanding of real magnetic materials.

Quantum spins arranged on a lattice and coupled to one another through magnetic interactions constitute a paradigmatic model system in condensed matter physics. Such systems produce a rich array of magnetically ordered ground states, such as paramagnets, ferromagnets and antiferromagnets. Certain geometries and interactions induce competition between these orderings in the form of frustration, resulting in spin liquids[1] and spin glasses[2], as well as phases with topological order[3]. Varying system parameters can induce quantum phase transitions between the various phases[4]. A deeper understanding of the competition and resulting transitions between magnetic phases would provide valuable insights into the properties of complex materials such as high-temperature superconductors[5], and more generally into the intricate behaviours that can emerge when many simple quantum mechanical objects interact with one another.

Studying quantum phase transitions of magnetic condensed matter systems is hindered by the complex structure and interactions present in such systems, as well as by the difficulty of controllably varying system parameters. With a few notable exceptions[6,7], these issues make it difficult to capture the physics of such systems with simple models. Accordingly, there is a growing effort under way to realize condensed matter simulators using cold atom systems[8,9], which are understood from first principles. The exquisite control afforded by cold atom experiments permits tuning of such systems through quantum phase transitions[9,10], thereby enabling investigations of criticality[11,12] and scaling[13]. Time-resolved local readout[14–16] and manipulation[17] provide direct access to local dynamics and correlations. With this powerful toolbox available, considerable attention has turned to understanding magnetic phase transitions using cold atom quantum simulations.

Initial experimental efforts to simulate quantum magnetism have focused on bulk itinerant systems of ultracold fermions[18] and small, highly connected spin-networks simulated with ion chains[19,20]. Polar molecules[21] and Rydberg atoms[22] have been the subject of preliminary investigations, both experimentally and theoretically[23–25], as alternatives to ground-state atoms with stronger, longer-range interactions. There has also been initial success in detecting ordered states, which are artificially prepared through patterned loading[17,26,27] and double-well experiments[28].

In this work, we simulate a one-dimensional chain of interacting Ising spins by using a Mott insulator[10,29,30] of spinless bosons in a tilted optical lattice[31]. Each Ising spin maps onto the motional degree of freedom of a single atom in the lattice. The more commonly considered approach instead represents the magnetic spins by two internal states of the atoms, with spin–spin interactions arising from super-exchange[32]. Super-exchange interactions in cold atoms are quite weak, though they have been successfully observed in double-well systems[33]. The approach presented here has the benefit of a dynamical timescale set by the tunnelling rate t, rather than by the super-exchange interaction t^2/U, where U is the on-site interaction energy. Combining the faster dynamics with the high spatial resolution afforded by a quantum gas microscope[14], we directly observe transitions between paramagnetic and antiferromagnetic phases as spin–spin interactions compete with magnetic fields.

One of the primary concerns in studying magnetism with ultracold atoms is the apparent difficulty of reaching the requisite temperatures[34–37]. Ultracold gases, however, are effectively isolated from their environment, and as such it is entropy and not temperature which is in principle conserved as system parameters are tuned. Spin-polarized Mott insulators have been demonstrated with defect densities approaching the per cent level[15,16], corresponding to configurational entropy far below the spin entropy required for magnetic ordering (see Supplementary Information). This allows us to use such a Mott insulator to initialize a magnetic system with low spin entropy. We engineer a magnetic Hamiltonian whose paramagnetic ground state overlaps well with the initial Mott state, and subsequently tune it through a quantum phase transition[38] to produce an antiferromagnet. The difficulty of cooling lattice spins is thus replaced with that of performing sufficiently slow ramps to minimize diabatic crossings of many-body energy gaps.

[1]Department of Physics, Harvard University, 17 Oxford Street, Cambridge, Massachusetts 02138, USA.

Ising interactions in a tilted optical lattice

The quantum Ising model is a textbook model of magnetism, and an Ising chain is one of the simplest many-body systems to exhibit a quantum phase transition. The Hamiltonian describing a one-dimensional antiferromagnetic Ising chain in the presence of an applied magnetic field is given by:

$$H = J\sum_i S_z^i S_z^{i+1} - h_z^i S_z^i - h_x^i S_x^i$$

Here $S_z^i(S_x^i)$ is the $z(x)$ spin-projection operator at site i, and $h^i{}_z(h^i{}_x)$ is the $z(x)$-component of the magnetic field applied to site i. The zero-temperature phase diagram of the model[39,40], shown in Fig. 1a for a homogeneous applied field (h_z,h_x), exhibits paramagnetism when applied fields dominate and antiferromagnetism when interactions dominate.

The approach to constructing a magnetic Hamiltonian that we use here was proposed in ref. 31 in the context of experiments reported in ref. 10, in which a gradient was applied to measure the insulating properties of the Mott state. In ref. 31 it was shown that under the influence of such field gradients, the dynamics of a one-dimensional Mott insulator map onto the aforementioned Ising model (see Methods) in the neighbourhood of $(h_z, h_x) = (1,0)$ (Fig. 1b).

In the Mott insulator regime ($U \gg t$), it is energetically forbidden for the atoms to tunnel if the tilt per lattice site, E, differs from the on-site atom–atom interaction U. Hence, the system remains in a state with one atom per lattice site while $E < U$ (Fig. 2a). As the tilt approaches the interaction strength ($E = U$), each atom is free to tunnel onto its neighbour, if that neighbour has not itself tunnelled (Fig. 2b). This nearest-neighbour constraint is the source of the effective spin–spin interaction. If the tilt E is increased sufficiently slowly through the transition to ensure that the system remains near the many-body ground state, density wave ordering results (Fig. 2c).

The mapping onto a spin-½ model arises as each atom has only two possible positions: an atom that has not tunnelled corresponds to an 'up' spin, and one that has, to a 'down' spin. Figure 2d shows the spin configurations corresponding to various atom distributions in the optical lattice. The transition from a uniform phase at small tilt to a density wave phase at large tilt then corresponds to a transition from a paramagnetic phase to an antiferromagnetic phase in the spin model. The longitudinal field h_z thus arises from the lattice tilt, and the transverse field h_x from tunnelling. The mapping between Bose–Hubbard and spin models (see Methods) is given by $(h_z,h_x) = (1-\tilde{\Delta},2^{3/2}\tilde{t})$, $\tilde{t} = t/J$, $\tilde{\Delta} = \Delta/J = (E-U)/J$, with $t = 10(4)$ Hz the single-particle tunnelling rate, $J \approx U = 413(19)$ Hz the constraint term, Δ the energy cost to tunnel, and $\tilde{t}$ and $\tilde{\Delta}$ the normalized tunnelling rate and tunnelling energy cost. Numbers in parentheses are 1σ uncertainties in measured quantities.

Spatially inhomogeneous tilts in the optical lattice can produce site-to-site variation of h_z, which affects the critical behaviour by inducing different sites to undergo the transition at different applied tilts. The resulting many-body energy gaps, dynamical timescales[41,42], and entropy of entanglement[43] then differ from the homogeneous case. Controlling such inhomogeneities is thus crucial for studies of magnetism.

Higher order processes can produce atom configurations that are not within the spin model (see Supplementary Information). We can thus study ground-state dynamics and low-energy excitations of the equivalent Ising model, but not high-energy excitations associated with adjacent 'down' spins. These restrictions admit investigation of the Ising physics only in the neighbourhood of the multicritical point $(h_z,\ h_x) \approx (1,\ 0)$. This regime is of particular theoretical interest because the model is here not exactly solvable[40]. It is nonetheless in the Ising universality class[31], and so a study of its critical physics would provide insight into the behaviours of the more commonly considered transverse ($h_z = 0$) Ising model.

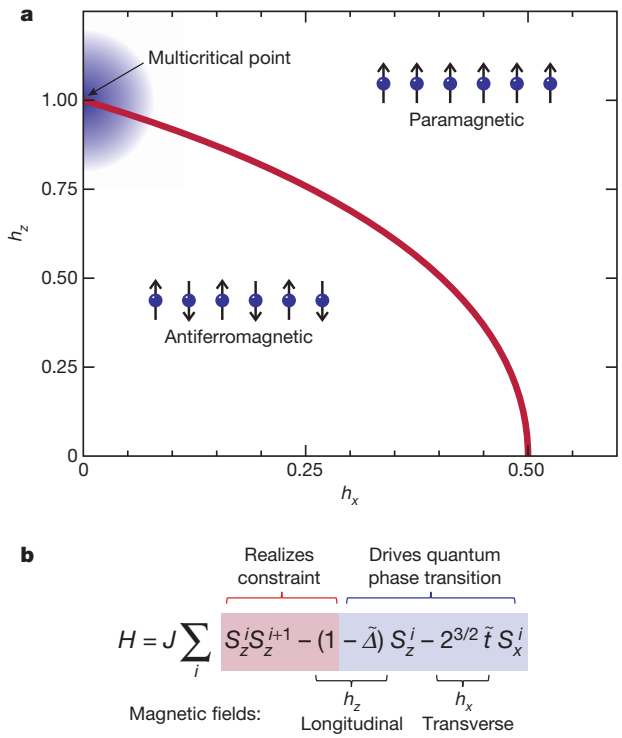

Figure 1 | Spin model and its phase diagram. a, An antiferromagnetic one-dimensional Ising chain in longitudinal (h_z) and transverse(h_x) magnetic fields exhibits two phases at zero temperature[39,40]: an antiferromagnetic phase in weak fields, and a paramagnetic phase in strong fields. These phases are separated by a second-order phase transition (red line), except at the multicritical point (h_z, h_x) = (1, 0), where the absence of quantum fluctuations produces a classical first-order transition. The region accessible in our experiment is highlighted in blue. **b**, Here the Hamiltonian may be decomposed into a constraint term (shaded red) that prevents adjacent 'down'-spins, and field terms (shaded blue) that drive the phase transition. See text for details.

Extracting spin observables

We detect magnetic ordering with single-site resolution by using our quantum gas microscope. The microscope is sensitive only to the parity of the site occupation number[14], and so paramagnetic domains (with one atom per lattice site) should appear as entirely bright regions, and antiferromagnetic domains (with alternating 0–2–0–2 occupation) as entirely dark regions. Within the resonant Hubbard subspace which maps to the spin model, the mean z-projection of spin may be related to odd-occupation probability at site i, $p^i{}_{\mathrm{odd}}$, according to (see Methods):

$$\overline{\langle S_z^i \rangle} = \frac{1}{2}\overline{p^i_{\mathrm{odd}}}$$

Here angle brackets denote realization-averages, and overbars region-averages.

Such an occupation measurement enables us to locally identify magnetic domains and estimate their size, but is not a direct measurement of the antiferromagnetic order parameter[31], and does not reflect the broken symmetry in the antiferromagnetic phase (see Methods). Accordingly, we also study the antiferromagnetic order parameter more directly through one-dimensional quantum noise interferometry[44].

Observing the phase transition

Our experiments begin with a Mott insulator of ^{87}Rb atoms in a two-dimensional optical lattice (with spacing $a = 680$ nm and a depth of $35E_r$, where E_r is the lattice recoil energy) in the focal plane of a high-resolution imaging system; this imaging system allows detection of single atoms on individual lattice sites, as described in previous work[14,15]. The value of E_r is given by $h^2/8ma^2$, where h is Planck's constant and m the mass of ^{87}Rb. We generate our effective h_z by tilting the lattice potential by E per lattice site, achieved by a magnetic

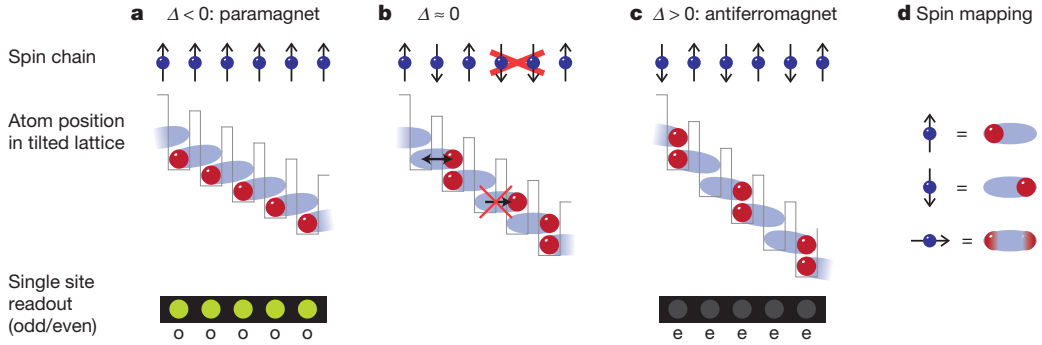

Figure 2 | Tilted Hubbard model and mapping to spin model. Consider first the middle row. **a**, When a Mott insulator is tilted by E per lattice site, it maintains unity occupancy until E reaches the on-site interaction energy U. **b**, As the energy cost to tunnel, $\Delta = E - U$, vanishes, an atom can tunnel to the neighbouring site if the atom on that site has not itself tunnelled. Otherwise, the tilt E inhibits tunnelling, producing a strong constraint. **c**, Tilting further, the system undergoes a transition into a doubly degenerate staggered phase. **d**, Here we show how this system maps onto interacting spin-½ particles, whose two spin states correspond to the two possible locations of each atom. The tunnelling constraint forbids adjacent down spins, realizing a spin–spin interaction. Top row: the initial Mott insulator corresponds to a paramagnet (**a**), the state at resonant tilt to an entangled (critical) spin configuration (**b**), and staggered ordering at large tilt to an antiferromagnet (**c**). Bottom row: parity-sensitive site-resolved imaging results in bright paramagnetic (**a**; o, odd), and dark antiferromagnetic (**c**; e, even) domains.

field gradient along the x direction (defined in Fig. 3A). We then prepare decoupled one-dimensional chains and null the harmonic confinement (see Methods). Finally we ramp (that is, increase) the lattice tilt, tuning the system across the transition at a fixed rate, and stop at various times to observe spin ordering.

We initiate the gradient ramp on the paramagnetic side of the phase transition (typically at $E/U = 0.7$), as the initial Mott state has good overlap with the paramagnetic ground state (Fig. 3A, a). At the end of the ramp ($E/U = 1.2$), we observe even occupation with probability 0.90(2) (Fig. 3A, b), as expected for an antiferromagnetic phase where the spin–spin interaction overwhelms the effective field h_z. In between, density-wave (antiferromagnetic) ordered regions begin to form, as shown in Fig. 3A, c. Figure 3C shows p_{odd} (averaged over 40 sites and 6 realizations) at various times during this ramp. A crucial characteristic of an adiabatic transition is that it is reversible. Figure 3B shows p_{odd} during a ramp from a paramagnetic phase to an antiferromagnetic phase and back in 500 ms. The recovery of the singly occupied sites is evidence of the reversibility of the process, and hence that the state after the forward ramp is an antiferromagnet.

We directly verify the existence of staggered ordering in the antiferromagnetic phase via a quantum noise correlation measurement[44] after a one-dimensional expansion (see Methods). The resulting one-dimensional spatial autocorrelation is plotted in Fig. 3D at both the beginning (Fig. 3D, a) and end (Fig. 3D, b) of the ramp from the paramagnetic phase to the antiferromagnetic phase. In the paramagnetic phase, the spectrum exhibits peaks at momentum difference $P = h/a$, characteristic of a Mott insulator[45]. In the antiferromagnetic phase, peaks appear at $P = h/2a$, indicating spatial ordering with twice the wavelength.

Single-site study of the transition

A high-resolution study reveals that in the presence of harmonic confinement the spins undergo the transition sequentially, owing to the resulting spatial variation of the effective longitudinal field. Figure 4a shows p_{odd} versus tilt for two rows of a harmonically confined Mott insulator, separated by seven lattice sites. That these rows tune through resonance at different tilts can be understood from the energy level diagram (Fig. 4b). We realize a homogeneous field Ising model by eliminating the harmonic confinement (see Methods) immediately before the slow ramp into the antiferromagnetic phase. The homogeneity is now only limited by residual lattice beam disorder, and accordingly, Fig. 4c demonstrates that different rows undergo the transition almost simultaneously, as anticipated theoretically (Fig. 4d).

After nulling the harmonic confinement, we use high-resolution imaging to study the transition on the single-site level. This allows us

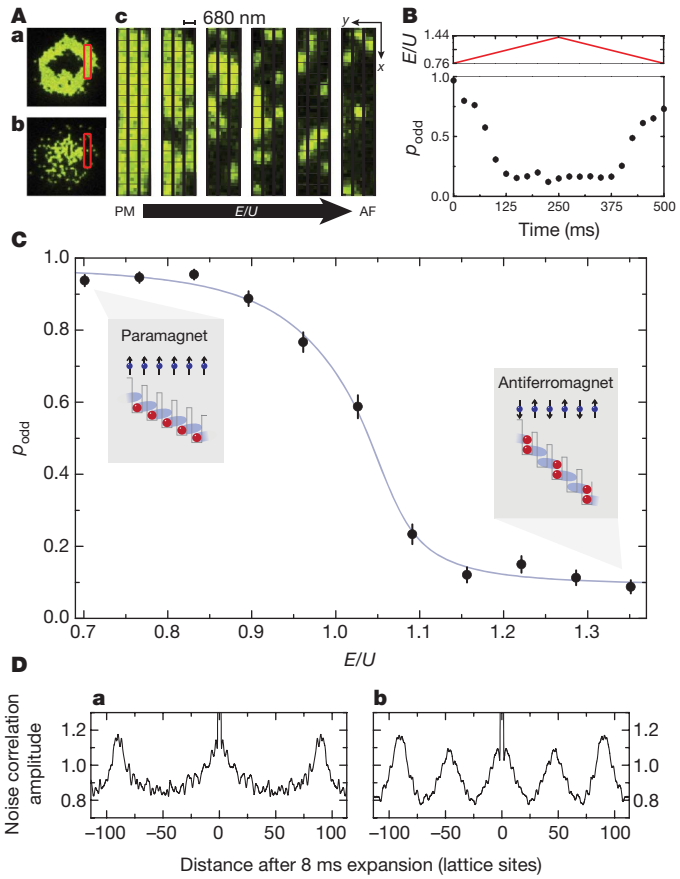

Figure 3 | Probing the paramagnet to antiferromagnet phase transition. **A**, Single-shot images as the tilt is swept through the phase transition in 250 ms. **A**, **a**, $n = 1$ (bright) and $n = 2$ (centre dark) Mott insulator shells in the paramagnetic (PM) phase. **A**, **b**, 'Inverted' shells characteristic of the staggered ordering of the antiferromagnetic (AF) phase. **A**, **c**, Several chains (red rectangles in **a** and **b**) of the $n = 1$ shell at various times during the sweep (left to right, in ms: 0, 50, 100, 150, 175, 250), showing antiferromagnetic domain formation. **B**, Demonstration of reversibility by tuning across the transition and back. Data points are p_{odd}, red line is tilt E/U, both versus time. **C**, A closer look at the paramagnetic to antiferromagnetic quantum phase transition in an $n = 1$ shell. Error bars, 1σ statistical errors in the region-averaged mean p_{odd}. Blue curve is a guide for the eye. Insets, state of the system at the beginning and end of the sweep. **D**, One-dimensional noise correlation measurement, with peaks at $P = h/a$ in the paramagnetic phase (**a**), and additional peaks at $P = h/2a$ in the antiferromagnetic phase (**b**).

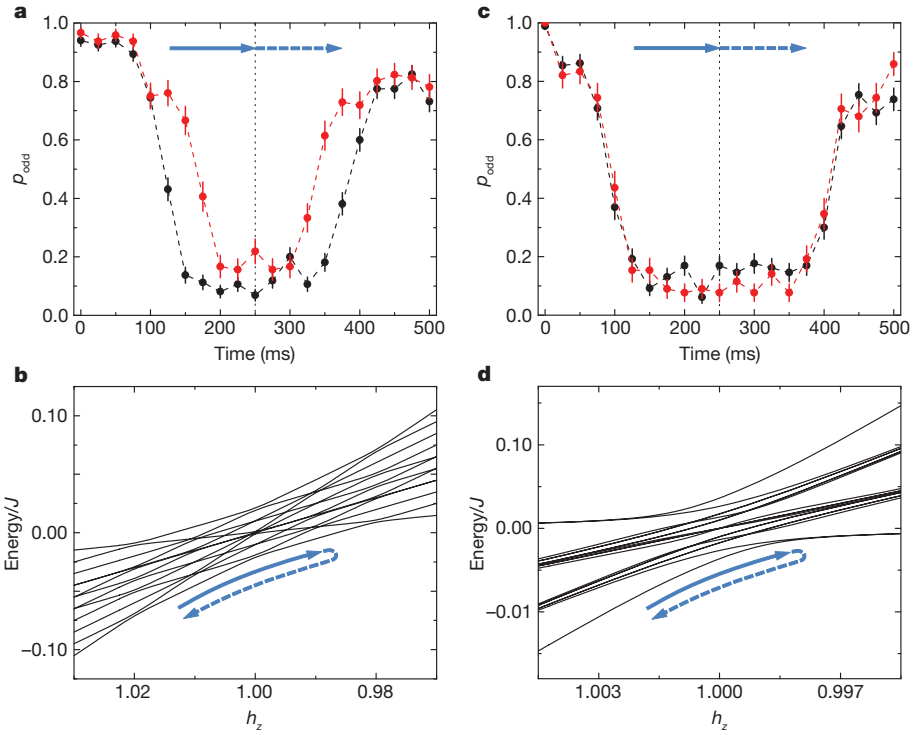

Figure 4 | Effect of harmonic confinement. **a**, For a ramp (in E/U; see Fig. 3B) across the transition and back in 500 ms, harmonic confinement broadens the transition region, inducing two rows (red and black data points) separated by seven lattice sites to go dark at different applied tilts. Red and black dashed lines are guides to the eye. **b**, Energy spectrum (black lines) of a one-dimensional Ising chain in a longitudinal field gradient (see Supplementary Information). Avoided crossings of the ground state correspond to single spin-flips. **c**, After nulling the confinement, the two rows undergo the transition together. **d**, Energy spectrum for a homogeneous chain. A single avoided crossing drives the many-body transition, whose gap scales inversely with system size. Solid and dashed blue arrows denote forward- and subsequent reverse-tilt ramps in all panels. Error bars are 1σ statistical uncertainties in the region-averaged mean of p_{odd}.

to focus on a single six-site chain with particularly low inhomogeneity, which we will study for the remainder of this Article. We identify such a chain by imaging individual lattice sites as the system is tuned across the paramagnetic–antiferromagnetic transition. Figure 5 shows the average occupation (over 43 realizations) of each of the six adjacent sites (black curves), versus tilt, as we ramp E/U across the transition. The r.m.s. variation in the fitted centres of the single-site transition curves (see Supplementary Fig. 1) is 6 Hz. This variation is significantly less than their mean 10–90% width of 105(30) Hz which corresponds to the effective transverse field $2^{3/2}t = 28(9)$ Hz. By quickly jumping across the transition with tunnelling inhibited, and then ramping slowly across the transition in reverse with tunnelling allowed (red curves in Fig. 5, taken under slightly different conditions), we are able to rule out large, localized potential steps that would otherwise prevent individual spins from flipping. The curves in Fig. 5 provide our best estimate of the inhomogeneity. However, exact determination of the site-to-site disorder using this technique is complicated by the many-body nature of the observed transition. New techniques, such as site-resolved modulation spectroscopy, would be necessary to ensure sufficient homogeneity for studies of criticality in long, uniform Ising chains.

Domain formation in a one-dimensional Ising chain

As the system is tuned through the transition by ramping E/U, quantum fluctuations induce the formation of antiferromagnetic domains, which appear as uninterrupted strings of dark lattice sites. Figure 6a shows the observed mean length-weighted dark domain length extracted from 43 single-shot images per tilt, as the system is tuned from the paramagnetic phase into the antiferromagnetic phase. The dark domain length is here defined as the number of contiguous dark sites in the previously identified homogeneous six-site chain (see Supplementary Information). The mean dark domain length reaches

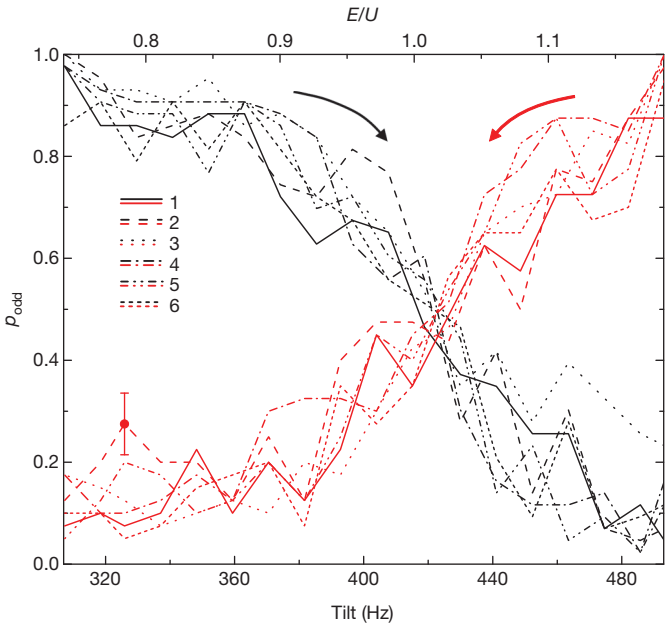

Figure 5 | Site-resolved transition in near-homogeneous Ising model. Shown is p_{odd} for six individual lattice sites forming a contiguous one-dimensional chain, plotted against the tilt, for both forward (black) and reverse (red) ramps of 250 ms. The spins are observed to undergo the transition at the same applied field to within the curve width, set by quantum fluctuations. Typical 1σ statistical error bar is shown. The reverse curve demonstrates the preparation of the highest-energy state of the restricted spin Hamiltonian, exhibiting paramagnetic ordering on the antiferromagnetic side of the transition, and antiferromagnetic ordering on the paramagnetic side.

4.9(2) sites, giving evidence that the average antiferromagnetic domain size approaches the system size.

We next investigate the effect of ramp rate on the transition from the paramagnetic phase into the antiferromagnetic phase in the homogeneous chain. The blue points in Fig. 6b show p_{odd} as a function of ramp speed across the transition, indicating qualitatively the fraction of the system that has not undergone transition into antiferromagnetic domains of any size. The time required to flip the spins is ~50 ms, consistent with tunnelling-induced quantum fluctuations driving the transition. The black points in Fig. 6b are the mean length-weighted dark domain length as a function of ramp rate, and approach the system size of six sites. The remaining defects probably result from heating during the ramp, and from initial defects of the Mott insulator (see Supplementary Information), as well as imperfect overlap of the initial Mott insulator with the paramagnetic state, which at initial tilt Δ_i is $1-O(t^2/\Delta_i^2)$.

Whereas the antiferromagnetic domain formation discussed thus far occurs in a system near its many-body ground state, we can also produce antiferromagnetic domains corresponding to the highest-energy state of the constrained Hilbert space. This is achieved by starting with the Mott insulator and rapidly ramping the field gradient through the transition point with tunnelling inhibited, then adiabatically ramping back with tunnelling permitted. This prepares a paramagnet on the antiferromagnetic side of the transition, then adiabatically converts it into an antiferromagnet on the paramagnetic side. The resulting data are shown in red in Figs 5 and 6a, demonstrating that these high-energy states are sufficiently long-lived to support domain formation. Similar ideas have been proposed for preparation of difficult-to-access many-body states using the highest energy states of Hamiltonians with easily prepared ground states[46].

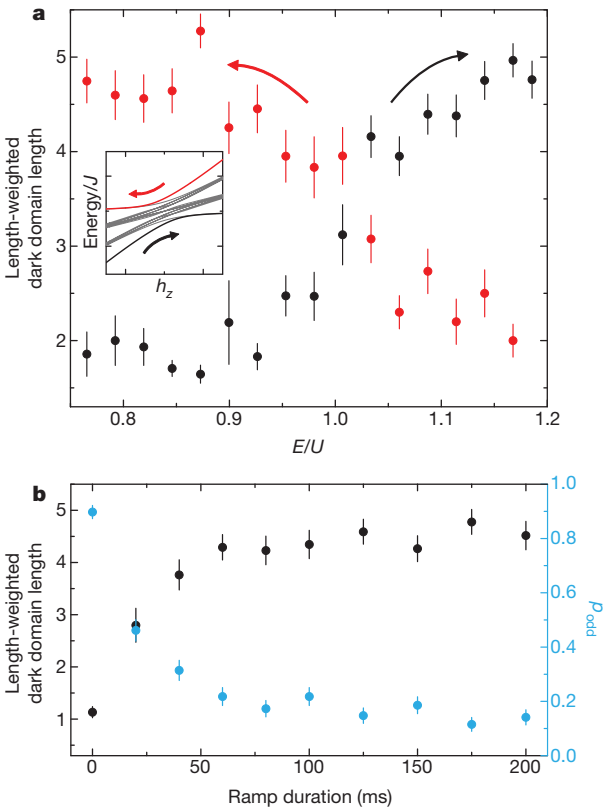

Figure 6 | Dynamics of antiferromagnetic domain formation. **a**, Within a single six-site chain with low disorder, the mean dark-domain length is plotted against tilt for forward (black) and reverse (red) ramps, as it grows to nearly the chain length. The reverse ramp produces antiferromagnetic domains on the paramagnetic side of the transition—corresponding to the highest-energy states of the spin Hamiltonian (inset). Arrows denote ramp direction. **b**, Within the same chain, p_{odd} (blue) and dark domain length (black) are plotted against ramp time from $E/U = 0.7$ to $E/U = 1.2$. Error bars for dark domain lengths are 1σ statistical uncertainties arising from the number of detected domains of each length; those for p_{odd} are 1σ statistical uncertainties in the mean.

Conclusions and outlook

We have experimentally realized a quantum simulation of an Ising chain in the presence of longitudinal and transverse fields. By varying the applied longitudinal field, we drive a transition between paramagnetic and antiferromagnetic phases, and verify the formation of spin domains via both direct *in situ* imaging and noise correlation in expansion. We study the adiabaticity requirements for transition dynamics, observing a timescale consistent with tunnelling-induced quantum fluctuations. By tuning rapidly through the transition and ramping back across it slowly, we prepare the highest-energy state of a many-body spin Hamiltonian.

We introduce and implement a novel route to studying low-entropy magnetism in optical lattices. Complexities associated with the cooling of spin mixtures[35–37] are circumvented by using a low-entropy, gapped Mott insulator as an initially spin-polarized state, and then adiabatically opening a spin degree of freedom[38]. The achieved entropies are so low that the residual tilt inhomogeneity, and not entropy, limits domain size. This recipe is directly applicable to more traditional approaches to quantum magnetism, including those using super-exchange interactions[33].

The spin-mapping demonstrated here realizes strong effective magnetic interactions, and opens new possibilities for studies of quantum magnetism and criticality. It will be interesting to investigate the effect of various types of controlled disorder on criticality and transition dynamics, as well as the possible existence of non-thermalizing states[47]. A particularly intriguing direction is the extension of the tilted Mott insulator physics to other models[48], and to higher dimensions. The square lattice geometry generates phases with longitudinal density wave ordering and transverse superfluidity[31]. More sophisticated geometries can induce frustration, resulting in novel phases such as quantum-liquids and valence-bond solids[49].

METHODS SUMMARY

We begin with a single-layer two-dimensional Mott insulator of ^{87}Rb atoms in a $35E_r$ lattice with 680-nm spacing as described in previous work. A magnetic field gradient along the x direction is ramped up to tilt the lattice. The lattice depth is then ramped to inhibit tunnelling transverse to the tilt, and to enhance tunnelling along the tilt. At the same time, the optical potential providing harmonic confinement is ramped down. The gradient is then ramped adiabatically through the transition point using a linear ramp. We can then perform either *in situ* imaging or a one-dimensional expansion of the chains to achieve noise correlation interferometry. In both cases, we use fluorescence imaging after pinning the atoms in a deep lattice to obtain the density distribution with single atom/single-lattice-site resolution. Fluorescence detection gives the atom number modulo 2 owing to light-assisted collisions of atoms on each lattice site during imaging.

Lattice depths are calibrated using Kapitza–Dirac scattering to 15%, however the width of single-site transition regions was found to be a more sensitive probe of the longitudinal tunnelling rate and hence of the longitudinal lattice depth (see Supplementary Fig. 1). The magnetic field gradient is calibrated using lattice modulation spectroscopy (see Supplementary Fig. 2).

We follow ref. 31 in mapping a one-dimensional Mott insulator of spinless bosons in a tilted lattice onto a chain of interacting dipoles (doublon-hole pairs, in a singly occupied Mott shell), and then onto a chain of spin-½ particles with antiferromagnetic Ising interactions in longitudinal and transverse fields.

Full Methods and any associated references are available in the online version of the paper at www.nature.com/nature.

Received 24 January; accepted 15 March 2011.
Published online 13 April 2011.

1. Balents, L. Spin liquids in frustrated magnets. *Nature* **464,** 199–208 (2010).
2. Binder, K. & Young, A. P. Spin glasses: experimental facts, theoretical concepts, and open questions. *Rev. Mod. Phys.* **58,** 801–976 (1986).

3. Kitaev, A. Anyons in an exactly solved model and beyond. *Ann. Phys.* **321,** 2–111 (2006).
4. Sachdev, S. *Quantum Phase Transitions* (Cambridge Univ. Press, 2001).
5. Anderson, P. W. The resonating valence bond state in La_2CuO_4 and superconductivity. *Science* **235,** 1196–1198 (1987).
6. Rüegg, C. *et al.* Quantum magnets under pressure: controlling elementary excitations in $TlCuCl_3$. *Phys. Rev. Lett.* **100,** 205701 (2008).
7. Coldea, R. *et al.* Quantum criticality in an Ising chain: experimental evidence for emergent E8 symmetry. *Science* **327,** 177–180 (2010).
8. Lewenstein, M. *et al.* Ultracold atomic gases in optical lattices: mimicking condensed matter physics and beyond. *Adv. Phys.* **56,** 243–379 (2007).
9. Bloch, I., Dalibard, J. & Zwerger, W. Many-body physics with ultracold gases. *Rev. Mod. Phys.* **80,** 885–964 (2008).
10. Greiner, M., Mandel, O., Esslinger, E., Haensch, T. W. & Bloch, I. Quantum phase transition from a superfluid to a Mott insulator in a gas of ultracold atoms. *Nature* **415,** 39–44 (2002).
11. Sachdev, S. Quantum magnetism and criticality. *Nature Phys.* **4,** 173–185 (2008).
12. Zhang, X., Hung, C.-L., Tung, S.-K., Gemelke, N. & Chin, C. Exploring quantum criticality based on ultracold atoms in optical lattices. Preprint at ⟨http://arXiv.org/abs/1101.0284⟩ (2010).
13. Hung, C.-L., Zhang, X., Gemelke, N. & Chin, C. Observation of scale invariance and universality in two-dimensional Bose gases. *Nature* **470,** 236–239 (2011).
14. Bakr, W. S., Gillen, J. I., Peng, A., Foelling, S. & Greiner, M. A quantum gas microscope for detecting single atoms in a Hubbard-regime optical lattice. *Nature* **462,** 74–77 (2009).
15. Bakr, W. S. *et al.* Probing the superfluid-to-Mott insulator transition at the single-atom level. *Science* **329,** 547–550 (2010).
16. Sherson, J. F. *et al.* Single-atom-resolved fluorescence imaging of an atomic Mott insulator. *Nature* **467,** 68–72 (2010).
17. Weitenberg, C. *et al.* Single-spin addressing in an atomic Mott insulator. *Nature* **471,** 319–324 (2011).
18. Jo, G. *et al.* Itinerant ferromagnetism in a Fermi gas of ultracold atoms. *Science* **325,** 1521–1524 (2009).
19. Friedenauer, A., Schmitz, H., Glueckert, J. T., Porras, D. & Schaetz, T. Simulating a quantum magnet with trapped ions. *Nature Phys.* **4,** 757–761 (2008).
20. Kim, K. *et al.* Quantum simulation of frustrated Ising spins with trapped ions. *Nature* **465,** 590–593 (2010).
21. Ni, K.-K. *et al.* A high phase-space-density gas of polar molecules. *Science* **322,** 231–235 (2008).
22. Saffman, M. & Walker, T. G. Quantum information with Rydberg atoms. *Rev. Mod. Phys.* **82,** 2313–2363 (2010).
23. Lukin, M. D. *et al.* Dipole blockade and quantum information processing in mesoscopic atomic ensembles. *Phys. Rev. Lett.* **87,** 037901 (2001).
24. Büchler, H. P. *et al.* Strongly correlated 2D quantum phases with cold polar molecules: controlling the shape of the interaction potential. *Phys. Rev. Lett.* **98,** 060404 (2007).
25. Weimer, H., Müller, M. & Lesanovsky, I. A Rydberg quantum simulator. *Nature Phys.* **6,** 382–388 (2010).
26. Lee, P. J. *et al.* Sublattice addressing and spin-dependent motion of atoms in a double-well lattice. *Phys. Rev. Lett.* **99,** 020402 (2007).
27. Soltan-Panahi, P. *et al.* Multi-component quantum gases in spin-dependent hexagonal lattices. *Nature Phys.* advance online publication doi:10.1038/nphys1916 (13 February 2011).
28. Fölling, S. *et al.* Direct observation of second-order atom tunnelling. *Nature* **448,** 1029–1032 (2007).
29. Fisher, M. P. A., Weichman, P. B., Grinstein, G. & Fisher, D. S. Boson localization and the superfluid-insulator transition. *Phys. Rev. B* **40,** 546–570 (1989).
30. Jaksch, D., Bruder, C., Cirac, J. I., Gardiner, C. W. & Zoller, P. Cold bosonic atoms in optical lattices. *Phys. Rev. Lett.* **81,** 3108–3111 (1998).
31. Sachdev, S., Sengupta, K. & Girvin, S. M. Mott insulators in strong electric fields. *Phys. Rev. B* **66,** 075128 (2002).
32. Duan, L. M., Demler, E. & Lukin, M. D. Controlling spin exchange interactions of ultracold atoms in optical lattices. *Phys. Rev. Lett.* **91,** 090402 (2003).
33. Trotzky, S. *et al.* Time-resolved observation and control of superexchange interactions with ultracold atoms in optical lattices. *Science* **319,** 295–299 (2008).
34. Capogrosso-Sansone, B., Soeyler, S. G., Prokof'ev, N. V. & Svistunov, B. V. Critical entropies for magnetic ordering in bosonic mixtures on a lattice. *Phys. Rev. A* **81,** 053622 (2010).
35. Weld, D. M. *et al.* Spin gradient thermometry for ultracold atoms in optical lattices. *Phys. Rev. Lett.* **103,** 245301 (2009).
36. Medley, P., Weld, D., Miyake, H., Pritchard, D. E. & Ketterle, W. Spin gradient demagnetization cooling of ultracold atoms. Preprint at ⟨http://arxiv.org/abs/1006.4674⟩ (2010).
37. McKay, D. & DeMarco, B. Cooling in strongly correlated optical lattices: prospects and challenges. Preprint at ⟨http://arxiv.org/abs/1010.0198⟩ (2010).
38. García-Ripoll, J. J., Martin-Delgado, M. A. & Cirac, J. I. Implementation of spin Hamiltonians in optical lattices. *Phys. Rev. Lett.* **93,** 250405 (2004).
39. Novotny, M. A. & Landau, D. P. Zero temperature phase diagram for the d=1 quantum Ising antiferromagnet. *J. Magn. Magn. Mater.* **54-57,** 685–686 (1986).
40. Ovchinnikov, A. A., Dmitriev, D. V., Krivnov, V. Y. & Cheranovskii, V. O. Antiferromagnetic Ising chain in a mixed transverse and longitudinal magnetic field. *Phys. Rev. B* **68,** 214406 (2003).
41. Imry, Y. & Ma, S.-k. Random-field instability of the ordered state of continuous symmetry. *Phys. Rev. Lett.* **35,** 1399–1401 (1975).
42. Dziarmaga, J. Dynamics of a quantum phase transition in the random Ising model: logarithmic dependence of the defect density on the transition rate. *Phys. Rev. B* **74,** 064416 (2006).
43. Vidal, G., Latorre, J. I., Rico, E. & Kitaev, A. Entanglement in quantum critical phenomena. *Phys. Rev. Lett.* **90,** 227902 (2003).
44. Altman, E., Demler, E. & Lukin, M. D. Probing many-body states of ultracold atoms via noise correlations. *Phys. Rev. A* **70,** 013603 (2004).
45. Fölling, S. *et al.* Spatial quantum noise interferometry in expanding ultracold atom clouds. *Nature* **434,** 481–484 (2005).
46. Sørensen, A. S. *et al.* Adiabatic preparation of many-body states in optical lattices. *Phys. Rev. A* **81,** 061603 (2010).
47. Bañuls, M. C., Cirac, J. I. & Hastings, M. B. Strong and weak thermalization of infinite nonintegrable quantum systems. *Phys. Rev. Lett.* **106,** 050405 (2011).
48. Plötz, P., Schlagheck, P. & Wimberger, S. Effective spin model for interband transport in a Wannier-Stark lattice system. *Eur. Phys. J. D.* doi:10.1140/epjd/e2010-10554-7 (2010).
49. Pielawa, S., Kitagawa, T., Berg, E. & Sachdev, S. Correlated phases of bosons in tilted, frustrated lattices. Preprint at ⟨http://arxiv.org/abs/1101.2897⟩ (2010).

Supplementary Information is linked to the online version of the paper at www.nature.com/nature.

Acknowledgements We thank E. Demler, W. Ketterle, T. Kitagawa, M.D. Lukin, S. Pielawa and S. Sachdev for discussions. This work was supported by the Army Research Office DARPA OLE programme, an AFOSR MURI programme, and by grants from the NSF.

Author Contributions All authors contributed to the construction of the experiment, the collection and analysis of the data, and the writing of the manuscript.

Author Information Reprints and permissions information is available at www.nature.com/reprints. The authors declare no competing financial interests. Readers are welcome to comment on the online version of this article at www.nature.com/nature. Correspondence and requests for materials should be addressed to M.G. (greiner@physics.harvard.edu).

METHODS

Mapping onto the spin model. We follow ref. 31 in formally mapping a one-dimensional Mott insulator of spinless bosons in a tilted lattice onto a chain of interacting dipoles (doublon-hole pairs, in a singly occupied Mott shell), and then onto a chain of spin-½ particles with antiferromagnetic Ising interactions in longitudinal and transverse fields. In a homogeneously tilted lattice, the one-dimensional Bose–Hubbard Hamiltonian reads:

$$H=-t\sum_j\left(a_j^\dagger a_{j+1}+a_j a_{j+1}^\dagger\right)+\frac{U}{2}\sum_j n_j(n_j-1)-E\sum_j jn_j$$

Here t is the nearest-neighbour tunnelling rate, U is the on-site interaction, E is the tilt per lattice site, $a_j^\dagger(a_j)$ is the creation (annihilation) operator for a particle on site j, and $n_j=a_j^\dagger a_j$ is the occupation number operator on site j.

For a tilt near $U=E$, the on-site interaction energy cost for an atom to tunnel onto its neighbour is almost precisely cancelled by the tilt energy. If one starts in a Mott insulator with M atoms per site, an atom can then resonantly tunnel onto the neighbouring site to produce a dipole excitation, with a pair of sites with $M+1$ and $M-1$ atoms. The resonance condition is only met if adjacent sites contain equal numbers of atoms, so only one dipole can be created per link and neighbouring links cannot both support dipoles. We define a dipole creation operator $d_j^\dagger=\frac{a_j a_{j+1}^\dagger}{\sqrt{M(M+1)}}$

The Bose–Hubbard Hamiltonian above can hence be mapped onto the dipole Hamiltonian:

$$H=-\sqrt{M(M+1)}t\sum_j\left(d_j^\dagger+d_j\right)+(U-E)\sum_j d_j^\dagger d_j$$

subject to the constraints $d_j^\dagger d_j\le 1, d_{j+1}^\dagger d_{j+1} d_j^\dagger d_j=0$

The factor of $\sqrt{M(M+1)}$ arises owing to bosonic enhancement.

To map from the dipole Hamiltonian to the spin-½ Hamiltonian, we define a link without (with) a dipole excitation to be an up (down) spin along $\hat{z}$. Then the creation/annihilation of dipoles are related to the flipping of spins, and we can write:

$$S_z^j=\tfrac{1}{2}-d_j^\dagger d_j,\ S_x^j=\tfrac{1}{2}\left(d_j^\dagger+d_j\right),\ \text{and}\ S_y^j=\tfrac{i}{2}\left(d_j^\dagger-d_j\right)$$

The constraint forbidding adjacent dipoles can be implemented by introducing a positive energy term $Jd_{j+1}^\dagger d_{j+1}d_j^\dagger d_j=J\left(S_z^{j+1}-\frac{1}{2}\right)\left(S_z^j-\frac{1}{2}\right)$ to the Hamiltonian, where J is of order U. This term gives rise to nearest-neighbour interactions and an effective longitudinal field for the spins.

Defining $\Delta=E-U$, the Hamiltonian for the spins now reads:

$$\begin{aligned}H&=J\sum_j S_z^j S_z^{j+1}-2\sqrt{M(M+1)}t\sum_j S_x^j-(J-\Delta)\sum_j S_z^j\\&=J\sum_j\left(S_z^jS_z^{j+1}-h_xS_x^j-h_zS_z^j\right)\end{aligned}$$

The dimensionless fields are defined as $h_x=2^{3/2}t/J=2^{3/2}\tilde{t}, h_z=\left(1-\frac{\Delta}{J}\right)=1-\tilde{\Delta}$, with M set to one as in our experiment.

Experimental details. Our experiments start with a single-layer two-dimensional Mott insulator of ^{87}Rb atoms in a $35E_r$ lattice with 680-nm spacing as described in previous work. The atoms are in the $|F=1, m_F=-1\rangle$ state and the initial fidelity of the Mott insulator is 0.95(2), with local fidelities as high as 0.98. A magnetic field gradient along the x direction is ramped up within 8 ms to tilt the lattice potential by $0.7U$ per lattice site, just below the transition point[31,40] at $E=U+1.85t$ ($h_z=1-0.66h_x$). At this point, the depth of the lattice along the chains is ramped down to $14E_r$, while the lattice transverse to the chains is ramped up to $45E_r$, within 2 ms. At the same time, the optical potential providing harmonic confinement is ramped down. Tunnelling between chains is negligible over the experimental timescale (see Supplementary Information for further discussion). The gradient is then ramped adiabatically through the transition point using a linear ramp that ends at a tilt of $1.2U$ per lattice site, typically within 250 ms.

We can then perform either an *in situ* measurement or a one-dimensional expansion of the chains to achieve noise correlation interferometry. In both cases, we use fluorescence imaging after pinning the atoms in a deep lattice to obtain the density distribution with single-atom/single-lattice-site resolution. Images far on the Mott side of the transition are used to select chains of atoms within the first shell of the insulator. The phase transition is then studied only within these chains, with quantitative curves using data only from the single chain with lowest disorder.

For noise correlation measurements, we first increase the lattice depth along the chains to $35E_r$ within 8 ms and then rapidly switch off that lattice to realize a one-dimensional expansion. Simultaneously with the lattice turn-off, the magnetic field gradient and the lattice along the chain are switched off, while the interchain lattice and the potential confining the atoms in the third direction remain on. After a one-dimensional expansion for 8 ms, the atoms are pinned for imaging. To extract information about density wave ordering in the chains, several hundred images (100 for paramagnetic phase, 300 for antiferromagnetic phase), each containing 15 chains, are fitted to extract the atom positions, and then spatially autocorrelated and averaged as described in ref. 45. In principle, the mean domain size can be extracted from the $P=h/2a$ peak width, however our peaks are broadened by finite expansion time and interactions during expansion, as well as aberration arising from the fact that the one-dimensional expansion is performed not in free space but in slightly corrugated confining tubes. Consequently domain size information is difficult to extract.

Lattice depths are calibrated to 15% using Kapitza–Dirac scattering, however the width of single-site transition regions was found to be a more sensitive probe of the longitudinal tunnelling rate and hence of the longitudinal lattice depth (see Supplementary Fig. 1), and accordingly was used throughout this Article.

The magnetic field gradient is calibrated using lattice modulation spectroscopy. In the presence of a potential gradient E per lattice site, modulation of the lattice depth along the chains causes resonant excitation at two frequencies, $U+E$ and $U-E$, corresponding to an atom in the Mott insulator moving up or down gradient. We detect these excitations as a reduction in the value of $p_{\rm odd}$ using *in situ* imaging (see Supplementary Fig. 2). Using the mean of the two resonances, we obtain the interaction energy $U=430(20)$ Hz at $16E_r$ longitudinal lattice, $45E_r$ transverse lattice (corresponding to $U=413(19)$ Hz at $14E_r$ longitudinal lattice, where the experiment operates, which agrees with a band-structure calculation of 401(25) Hz). The separation between the resonances as a function of applied gradient is used to calibrate E. At zero applied magnetic field gradient, we find the stray gradients to be less than $0.02U$.

Local and long-range observables. *In situ* detection gives the atom number modulo 2, owing to light-assisted collisions of atoms on each lattice site during imaging. In the spin language, the detection parity operator P_i measures the spin–spin correlation between adjacent spins:

$$P_i=4S_z^{i-1}S_z^i$$

The probability that site i has odd occupation is given by $p_{\rm odd}^i=\frac{1}{2}(1+\langle P_i\rangle)$, where angle brackets denote realization averages. This is then related to the spin observables in the effective model by $\left\langle S_z^{i-1}S_z^i\right\rangle=\frac{1}{2}\left(p_{\rm odd}^j-\frac{1}{2}\right)$. We average over all the atoms in a region to obtain $p_{\rm odd}=\overline{p_{\rm odd}^j}$, which, in combination with the constraint that neighbouring down spins are not allowed, enables us to relate the region-averaged mean z-projection of spin to $p_{\rm odd}$ according to: $\overline{\left\langle S_z^j\right\rangle}=\frac{p_{\rm odd}}{2}$. This quantity varies smoothly across the transition and depends only weakly on the chain length. On the other hand, the order parameter for the transition $O=\left\langle\left(\frac{1}{N}\sum_j(-1)^jS_z^j\right)^2\right\rangle$ depends on the chain length (Supplementary Fig. 3) and is non-analytic across the transition for a thermodynamic system.

The amplitude of the noise correlation signal at separation d for a chain consisting of a large number of atoms is $C(d)=1+\frac{1}{N^2}\left|\sum_j e^{-i\frac{madj}{\hbar t}}n_j\right|^2$ where N is the number of lattice sites, j is the lattice site index, a is the lattice spacing, m is the mass of the atom, t is the expansion time, n_j is the occupation of the jth site, and $\hbar$ is $h/2\pi$. It can be shown that the correlation signal at $d=\frac{\pi\hbar t}{ma}$ is related to the order parameter $O=C\left(\frac{\pi\hbar t}{ma}\right)-1$.

The finite chain length in the chains reduces the baseline of the correlation signal from 1 by an amount of the order of $1/N$.